Unusual thermoelectric properties of $BaFe_2As_2$ in high magnetic fields

M. Meinero,[1,2] F. Caglieris,[3] G. Lamura,[2] I. Pallecchi,[2] A. Jost,[4] U. Zeitler,[4] S. Ishida,[5] H. Eisaki,[5] and M. Putti[1,2]

[1]*Dipartimento di Fisica, Università di Genova, Via Dodecaneso 33, 16146 Genova, Italy*

[2]*CNR-SPIN, Corso Perrone 24, 16152 Genova, Italy*

[3]*IFW Dresden, Helmholtz Strasse 33, Dresden, Germany*

[4]*High Field Magnet Laboratory (HFML-EMFL), Radboud University, Toernooiveld 7, 6525ED Nijmegen, The Netherlands*

[5]*National Institute of Advanced Industrial Science and Technology, Tsukuba 305-8568, Japan*

(Received 15 June 2018; published 8 October 2018)

Electric and thermoelectric transport properties are mutually intertangled in diffusive transport equations. In particular, in high mobility multiband systems an anomalous behavior may occur, which can be tracked down to the properties of the individual bands. Here, we present magnetoelectric and magnetothermoelectric transport properties of a $BaFe_2As_2$ high-quality single crystal, for different magnetic field directions up to 30 T. We detect a giant Nernst effect and an anomalous field dependence of the Seebeck coefficient. The extraction of the Peltier tensor coefficients α_{xx}, α_{xy}, and α_{xz} allows us to disentangle the main transport mechanisms in play. The large α_{xy} and α_{xz} values and their field dependence provide evidence of the presence of a high mobility band, compatible with a Dirac dispersion band, crossing the Fermi level, and suggest a possible three-dimensional nature of the Dirac fermions.

DOI: 10.1103/PhysRevB.98.155116

I. INTRODUCTION

The mutual entanglement of electric and thermoelectric properties in diffusive transport equations is a well-established framework of condensed matter physics. Yet, the application of this formalism in its entirety to real materials has not been thoroughly exploited so far, leaving this powerful investigation tool underused in its full potential. Real materials may exhibit multiband character (with linear and parabolic dispersion), anisotropic electronic structure, and physical mechanisms other than diffusive motion of carriers, all of which make the combined analysis of transport properties highly challenging. On the other hand, each of these factors yields peculiar features in the temperature and field dependence of transport properties, thus allowing the extraction of individual band parameters such as, for instance, the signature of linearly dispersing bands at the Fermi level.

The experimental discovery of topological Dirac and Weyl semimetals has recently boosted the investigation of Dirac fermions (DFs) in condensed matter physics [1,2]. They have been investigated in different two-dimensional systems [3,4] and in the surface states of topological insulators [5,6] but they rarely appear in the bulk of three-dimensional (3D) solids [7–9]. The parent compounds of the iron-arsenide superconductors represent one of the rare 3D crystal solid systems in which DFs are claimed to exist in a magnetic ground state [7,10]. These compounds exhibit indeed a collinear antiferromagnetic (AFM) order below a certain temperature, slightly anticipated by a structural transition from a tetragonal to an orthorhombic symmetry [10]. Theoretical calculations in the AFM state [11] show the presence of topologically protected Dirac cones with linear energy-momentum dispersion carrying the same chirality. Indeed, DFs have been experimentally revealed in $BaFe_2As_2$ by angle resolved photoemission spectroscopy (ARPES) measurements [12,13], linear magnetoresistance [14–16], and very recent infrared studies [7]. A nontrivial topology has been also found in other families, such as in the 1111 family, where a finite Berry phase has been observed in the CaFeAsF compound through quantum oscillations [17]. Moreover, the presence of topologically protected DFs should cause a significantly suppressed intraband scattering rate in Dirac bands, even if the strong multiband scattering related to Fermi-surface nesting masks any effect of Dirac cone chirality in the measured transport. Thermoelectric transport, although very informative, is much less analyzed. A giant Nernst effect, which is typical of the iron-based parent compounds, has been described in terms of the presence of Dirac cones [11,18,19] but a coherent analysis of all the relevant mechanisms in play is still lacking.

In this paper, we report a detailed experimental study of the magnetoelectric and magnetothermoelectric transport properties of a $BaFe_2As_2$ single crystal, the mobility of which is enhanced by proper thermal annealing in the preparation method. Thanks to the high mobility, this semimetal exhibits signatures of its electronic structure, which can be extracted by disentangling different contributions to magnetotransport. Indeed, we find that the Seebeck and Nernst coefficients measured up to very high magnetic fields (B) exhibit a peculiar B dependence, which points to the existence of high mobility carriers compatible with the DF scenario.

II. EXPERIMENTAL DETAILS

The $BaFe_2As_2$ single crystal was grown by the self-flux method, as described in [20]. The crystal was cut in a rectangular shape along the tetragonal [110] directions, which become the a or b axes in the orthorhombic phase if uniaxial pressure is applied to the sample [21]. The crystal dimensions

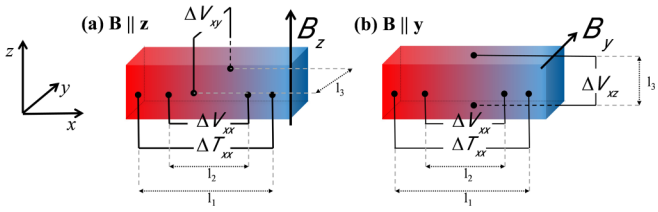

FIG. 1. Thermoelectric measurements setup. A thermal gradient ΔT_{xx} was generated along x and a longitudinal voltage ΔV_{xx} was detected with B applied (a) along z and (b) along y. The Seebeck effect in both cases is defined as $S_{xx} = (\Delta V_{xx}/\Delta T_{xx})(l_1/l_2)$. In (a), a transverse voltage ΔV_{xy} is detected along y and the Nernst effect is defined as $N_{xy} = (\Delta V_{xy}/\Delta T_{xx})(l_1/l_3)$. In (b) a transverse voltage ΔV_{xz} is measured along z and the Nernst effect is defined as $N_{xz} = (\Delta V_{xz}/\Delta T_{xx})(l_1/l_3)$.

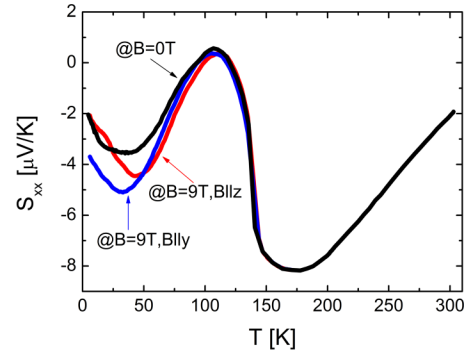

FIG. 2. Seebeck effect measured from 5 to 300 K in a magnetic field of 0 T (black curve) and 9 T $\|z$ (red curve) and $\|y$ (blue curve).

were $2.5 \times 0.8 \times 0.7\,\mathrm{mm}^3$, with the shortest edge along the c axis. In the following we will use the notations x, y, and z to indicate the geometrical sides of our slablike sample. Since in the orthorhombic phase no uniaxial pressure was applied to the sample, the crystal presented the expected in-plane twin domains so that we cannot refer x and y to the orthorhombic a and b axis, whereas the z direction corresponds to the c axis. The crystal was sealed into an evacuated quartz tube together with BaAs powders and annealed at 800 °C for two days. Such annealing significantly improves the electrical transport properties by removing the lattice defects and enhancing the carrier mobilities [20]. The good quality of the crystal was confirmed by magnetic susceptibility measurement and by the high residual resistivity ratio, defined as ρ (300 K)/ρ (5 K), which is around 27 [22].

Seebeck effect, magnetoresistance, and Hall effect measurements were performed in the temperature range from 5 to 300 K and in magnetic fields up to 9 T using a physical property measurement system (Quantum Design). High magnetic field thermoelectric characterizations were performed up to 30 T at the High Field Magnet Laboratory in Nijmegen.

In order to probe the B dependence of the thermoelectric coefficients, the measurements were performed using two different configurations, varying the orientation of B. Figure 1 shows the experimental setup and a sketch of the measured quantities which allow obtaining the thermoelectric coefficients.

We performed all the measurements with both positive and negative B in order to separate the even and odd parts of the signal with respect to the magnetic field.

It is worth noting that a partial detwinning by action of in-plane magnetic field has been observed in a Co-doped $BaFe_2As_2$ crystal [23]. A partial detwinning is therefore expected in our case when $B\|y$. We will discuss this point in the next paragraphs.

III. RESULTS AND DISCUSSION

Figure 2 shows the S_{xx} coefficients in the temperature range between 5 and 300 K in 0- and 9-T magnetic fields, applied $\|z$ and $\|y$. At room temperature, zero-field S_{xx} is negative and its absolute value increases linearly with decreasing temperature, reaching the maximum value of about $-8\,\mu\mathrm{V\,K}^{-1}$ around $T = 175$ K. In correspondence with the structural/magnetic transition at $T_N = 140$ K an abrupt change occurs: The signal strongly diminishes and crosses zero around $T = 120$ K. For $T = 90$ K, S_{xx} becomes negative again and it exhibits a broadened minimum centered around 40 K. This behavior is in substantial agreement with previous reports on $BaFe_2As_2$ [24–27].

No magnetic field dependence is detected in the paramagnetic state ($T > T_N$) whereas in the AFM state ($T < T_N$) we observe two different B behaviors when $B\|z$ or $B\|y$. In both cases the magnetic field tends to increase S_{xx} by up to 30 and 50% of the zero-field signal for $B\|z$ and $B\|y$, respectively. The main difference between the two curves is indeed the position of their negative maxima, which is around $T = 30$ and 50 K, respectively, revealing the possible competition of different mechanisms in play.

In order to investigate this peculiar field dependence, we measured S_{xx} as a function of B up to 30 T for selected temperatures in the AFM regime. Figures 3(a) and 3(c) show $\Delta S_{xx}(B) = S_{xx}(B) - S_{xx}(0)$ with magnetic field applied $\|z$ or $\|y$, respectively. In Fig. 3(a), $\Delta S_{xx}(B)$ has an absolute value of the order of several microvolts per degree Kelvin at the largest field, is nonmonotonic, and presents a sign change from negative to positive which shifts to higher field with increasing temperature. This trend completely changes for $B\|y$ [Fig. 3(d)], where $\Delta S_{xx}(B)$ remains negative up to 30 T. In Figs. 3(b) and 3(d) we show the Nernst coefficients N_{xy} and N_{xz} measured up to 30 T for $B\|z$ and $B\|y$, respectively. The former varies almost linearly with magnetic field, reaching a maximum value of 30 μV/K [Fig. 3(b)] at the maximum field, whereas the latter exhibits a slightly superlinear magnetic field dependence, reaching a maximum value of 13 μV/K [Fig. 3(e)]. (See the Supplemental Material [22] for the temperature dependence of $\nu = N_{xy}/B$.)

Before discussing in detail these data, we consider here the possible effects due to the partial detwinning expected for $B\|y$, particularly relevant for the present system because of the in-plane anisotropy of its Seebeck coefficient [28]. We estimated that this effect produces a maximum increase of S at 30 K and 15 T of about 0.1 μV/K [29]. This is opposite in sign and negligible in magnitude with respect to the value of $\sim$1.5 μV/K, measured in the same conditions. Furthermore, no effect on the Nernst coefficient is expected [29].

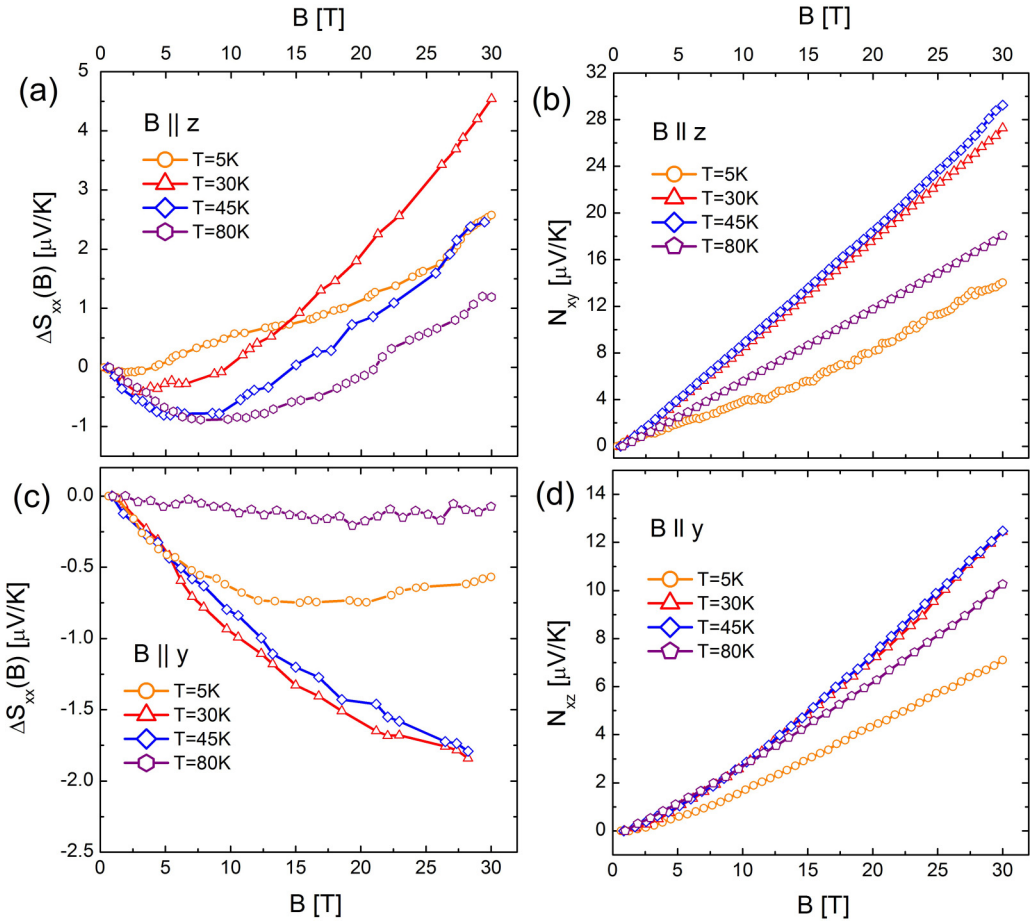

FIG. 3. $\Delta S_{xx}(B)$ measured at $T = 5,\ 30,\ 45$, and 80 K for B up to 30 T applied $\|z$ (a) and $\|y$ (c). Nernst coefficients N_{xy} (b) and N_{xz} (d) measured at $T = 5,\ 30,\ 45$, and 80 K for B up to 30 T.

In Figures 4(a) and 4(c) we report the magnetoresistance $\Delta\rho/\rho = [\rho_{xx}(B)-\rho_{xx}(0)]/\rho_{xx}(0)$ measured up to 9 T for $B\|z$ and $B\|y$, respectively. At $T = 5$ K, it reaches 160% for $B\|z$ and 130% for $B\|y$. In this case, the effect due to the detwinning for $B\|y$ is negligibly small and can be evaluated as low as 0.7% at 4 K and 15 T [30]. For both the field directions the $\Delta\rho/\rho$ versus B curves cannot be described just by a quadratic term representing the classical contribution [31]. Instead, an additional linear term is needed, in agreement with previous reports [14,15,20]. In pnictides, this linear behavior has been attributed to the presence of Dirac cones in the band structure. In Figs. 4(b) and 4(d) we show the magnetic field dependence of the Hall resistivities ρ_{xy} and ρ_{xz} measured up to 9 T for selected temperatures in the range 5–80 K, for $B\|z$ and $B\|y$, respectively. R_H versus T [reported in the inset of Fig. 4(b)], evaluated in the low-field limit, appears to be similar in the two configurations. However, it is worth noting that ρ_{xy} and ρ_{xz} B dependences look pretty different, as one could expect for an anisotropic material [32]. ρ_{xy} soon deviates from B-linear dependence and shows a broad minimum below 9 T. Remarkably, ρ_{xy} of a twin sample of literature ($BaFe_2As_2$ crystal annealed at 800 °C for two days) measured up to 15 T exhibits a change in sign above 9 T [20]. In contrast to ρ_{xy}, ρ_{xz} shows only a slight sublinear B dependence.

S_{ii} and N_{ij} can be expressed in terms of the electric conductivity tensor $\boldsymbol{\sigma}$ and the Peltier tensor $\boldsymbol{\alpha}$ as follows:

$$S_{ii} = \alpha_{ii}\frac{\sigma_{ii}}{\sigma_{ii}^2+\sigma_{ij}^2} + \alpha_{ij}\frac{\sigma_{ij}}{\sigma_{ii}^2+\sigma_{ij}^2} = \alpha_{ii}\rho_{ii} + \alpha_{ij}\rho_{ij}, \quad (1)$$

$$N_{ij} = -\alpha_{ii}\frac{\sigma_{ij}}{\sigma_{ii}^2+\sigma_{ij}^2} + \alpha_{ij}\frac{\sigma_{ii}}{\sigma_{ii}^2+\sigma_{ij}^2} = -\alpha_{ii}\rho_{ij} + \alpha_{ij}\rho_{ii} \quad (2)$$

where in the second equalities we introduce the resistivity tensor $\boldsymbol{\rho} = \boldsymbol{\sigma}^{-1}$. Remarkably, Eqs. (1) and (2) remain valid also for multiband materials, where the single transport coefficients are simply replaced by the sum over the different bands [33]. Both S_{ii} and N_{ij} are composed of two terms. In the longitudinal S_{ii} coefficient [Eq. (1)] the diagonal entries of $\boldsymbol{\rho}$ and $\boldsymbol{\alpha}$ multiply each other in the first term while the off-diagonal ones combine together in the second term. In the transversal N_{ij} coefficient [Eq. (2)] diagonal and off-diagonal entries are mixed up. It is worth noting that the off-diagonal entries represent the diffusive transverse transport coefficients, which rise up only in the presence of a Lorentz force acting on charge carriers. In the case of $B = 0$ this leads to $S_{ii} = \alpha_{ii}\rho_{ii}$ and $N_{ij} = 0$. If $B \neq 0$, in the great majority of the conducting materials $\rho_{ii} \gg \rho_{ij}$ and $\alpha_{ii} \gg$

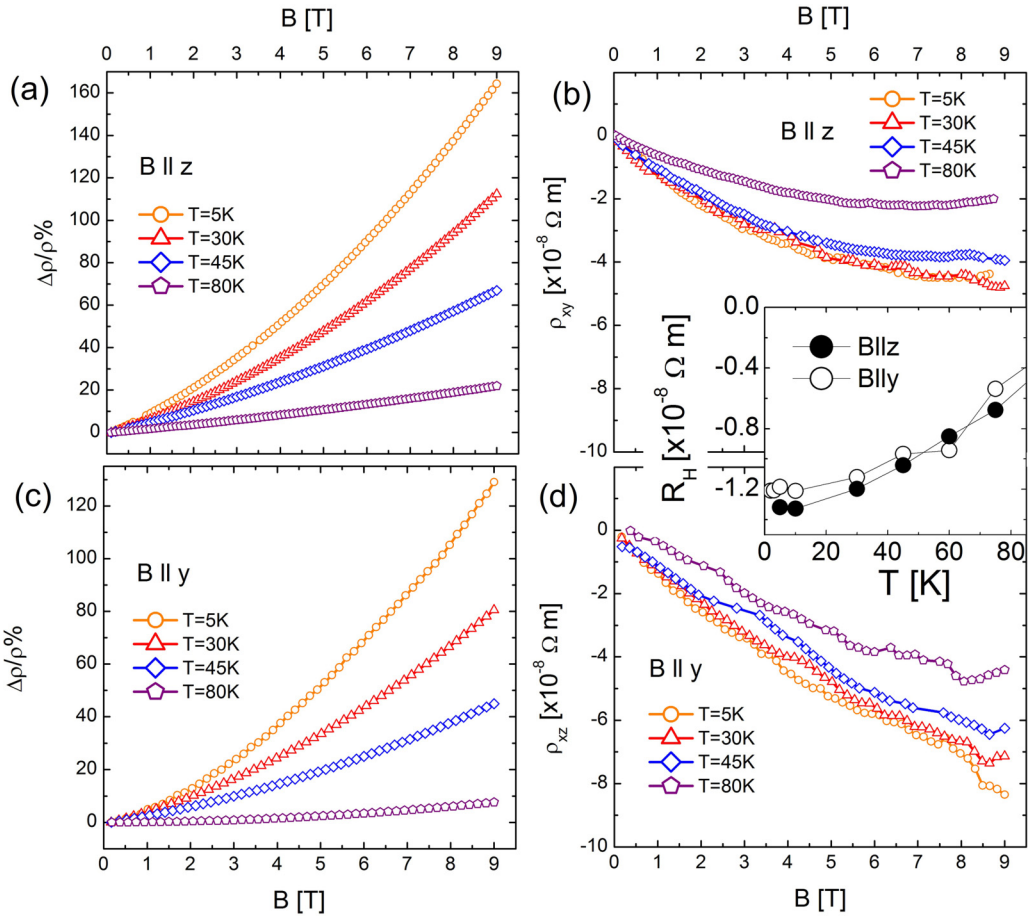

FIG. 4. $\Delta\rho/\rho\%$ measured at $T = 5,\ 30,\ 45$, and 80 K for B up to 9 T applied $\|z$ (a) and $\|y$ (c). ρ_{xy} (b) and ρ_{xz} (d) measured at $T = 5,\ 30,\ 45$, and 80 K for B up to 9 T. Inset of (b): R_H vs T in the temperature range 0–80 K when B is $\|z$ (filled dots) and $\|y$ (empty dots). R_H curves up to 250 K are reported in [22].

α_{ij}, namely, the longitudinal transport coefficients are much larger than their transverse counterparts. Hence, it is typically verified that $\alpha_{ii}\rho_{ii} \gg \alpha_{ij}\rho_{ij}$, bringing a negligible contribution of the second term $\alpha_{ij}\rho_{ij}$ in Eq. (1) to the Seebeck coefficient even in finite magnetic field [34]. Furthermore, in conventional metals, N_{ij} is usually very small (in the range of nanovolts per degree Kelvin) due to Sondheimer's cancellation [35].

In addition, the transverse transport coefficients are B linear in the low-field limit ($\mu B \ll 1$, where μ is the charge carriers' mobility) whereas their longitudinal counterparts generally show a negligible B dependence [36]. However, the term $\alpha_{ii}\rho_{ii}$ may have nondiffusive contributions with a sizeable B dependence; among these is the magnon drag contribution in magnetic materials [37–39].

In the light of these considerations, the giant N_{ij} combined with a large field dependence of S_{ii} in the antiferromagnetic phase of $BaFe_2As_2$ are the fingerprints of the strong departure from a conventional behavior. In the following we propose an analytical approach in order to single out the leading terms that cause anomalous contributions and identify the physical mechanisms that play a key role.

By combining the experimental values of resistivity tensor entries, $\rho_{ii}(B)$ and $\rho_{ij}(B)$, and thermomagnetic coefficients, S_{ii} and N_{ij}, the Peltier coefficients α_{ii} and α_{ij} are derived by solving Eqs. (1) and (2) for α_{ii} and α_{ij}:

$$\alpha_{ii} = \frac{S_{ii}\rho_{ii} - N_{ij}\rho_{ij}}{\rho_{ii}^2 + \rho_{ij}^2}, \tag{3}$$

$$\alpha_{ij} = \frac{S_{ii}\rho_{ij} + N_{ij}\rho_{ii}}{\rho_{ii}^2 + \rho_{ij}^2}. \tag{4}$$

Note that according to our experimental setup (Fig. 1) the subscript i is identified with x and the subscript j is identified with y when $B\|z$, whereas i corresponds to x and j corresponds to z when $B\|y$.

In order to estimate α_{ii} and α_{ij} up to high fields, we extrapolated our magnetoresistance data [Figs. 4(a) and 4(c)] up to 30 T assuming that no saturation occurs in that range, as it was observed up to 55 T for the same compound in [40] and up to 30 T for a parent compound of the 1111 family in [41].

Furthermore, since ρ_{xy} and ρ_{xz} show a nontrivial B dependence which does not disclose up to 9 T, it is not possible to extrapolate univocally our data [Figs. 4(b) and 4(d)] up to 30 T. However, to study the $B\|z$ configuration we extrapolated up to 30 T the ρ_{xy} data measured up to 15 T in the twin sample of [20].

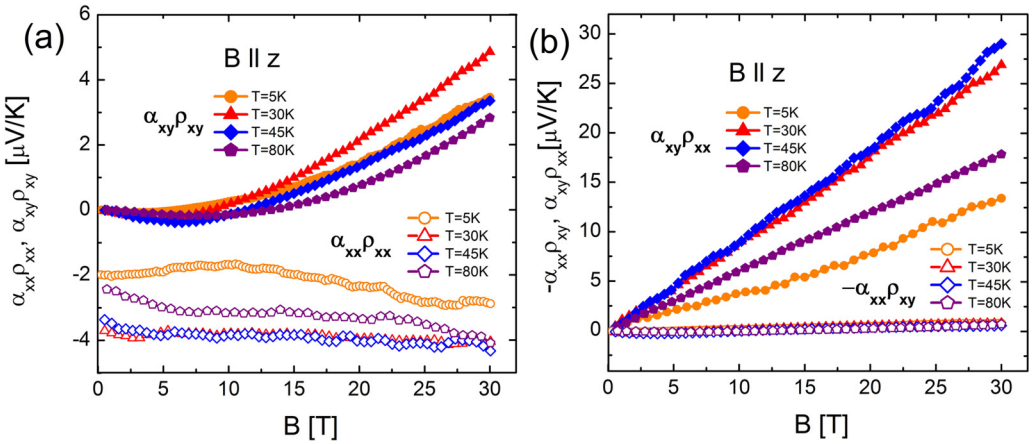

FIG. 5. (a) $\alpha_{xy}\rho_{xy}$ (filled symbols) and $\alpha_{xx}\rho_{xx}$ (empty symbols) vs B up to 30 T for selected temperatures in the range 5–80 K. (b) $\alpha_{xy}\rho_{xx}$ (filled symbols) and $-\alpha_{xx}\rho_{xy}$ (empty symbols) vs B up to 30 T for selected temperatures in the range 5–80 K.

Thus, we focus on the $B\|z$ configuration. In Fig. 5, we show the results of our analysis for selected temperatures in the range 5–80 K. In Figs. 5(a) and 5(b) we compare the two terms in Eqs. (1) and (2) which compose S_{xx} and N_{xy}, respectively. Figure 5(a) compares the field dependence of $\alpha_{xx}\rho_{xx}$ with $\alpha_{xy}\rho_{xy}$ up to 30 T.

The $\alpha_{xx}\rho_{xx}$ curves look almost flat at all temperatures. This term would include magnon drag contribution, however in AFM materials an external magnetic field strongly enhances the magnon drag contribution to S_{xx} only if it is applied as parallel to the easy axis of the magnetic order, while its effect should be minimal if applied perpendicularly [38]. In the case of $BaFe_2As_2$ the easy axis lies in the ab plane; this means that negligible contribution from the magnon drag is expected when $B\|z$.

In contrast, $\alpha_{xy}\rho_{xy}$ versus B, after an initial decrease, increases rapidly with positive sign up to 30 T, emerging as the principal responsible for the large field dependence of S_{xx} in this measurement configuration. In more detail, the sign of $\alpha_{xy}\rho_{xy}$ is driven by the unusual change from negative to positive sign of ρ_{xy} at high B [20]. Since $|\rho_{xx}| > |\rho_{xy}|$ [22], the predominance of $\alpha_{xy}\rho_{xy}$ is induced by an anomalously high α_{xy}.

In Fig. 5(b) the two terms which compose N_{xy} are plotted and it is evident that $|\alpha_{xy}\rho_{xx}| > |\alpha_{xx}\rho_{xy}|$, which is to say that $\alpha_{xy}\rho_{xx}$ is also responsible for the giant N_{xy}. Figure 6 reports the field dependence of α_{xy} estimated as in Eq. (4) up to 30 T for selected temperatures in the range 5–80 K. Remarkably, a nonmonotonic behavior emerges: all the $\alpha_{xy}(B)$ curves exhibit a maximum which is shifted to higher fields with increasing temperature.

Although a quantitative expression of α_{xy} in terms of microscopic parameters is challenging, in a single-band scenario it can be obtained from the Mott relation that [42]

$$\alpha_{xy} = A\mu^2 B/[1 + (\mu B)^2] \tag{5}$$

where μ is the carrier mobility and $A = c\pi^2 k_B^2 T n/E_F$ with k_B being the Boltzmann constant, n the carrier density, E_F the Fermi energy, and c a coefficient of the order of unity depending on the dimensionality of the system [43] and on the details of the energy dependence of σ_{xy} [42].

Without providing a quantitative description, Eq. (5) gives a qualitative understanding of the particular conditions from which a sizeable α_{xy} emerges. High μ and small E_F are required, namely, tiny pockets in the Fermi surface with small effective masses can significantly contribute. Furthermore, it is noteworthy that the above formulation does not depend on the carrier sign, which means that in the case of multiband materials contributions from holelike and electronlike pockets add up and the one coming from a band with high μ and small E_F emerges. We interpolate our $\alpha_{xy}(B)$ data using Eq. (5) as a fitting function (dashed black lines in Fig. 6), finding a good agreement with the experimental data. We extract the mobility μ as a fit parameter, obtaining values up to 10^3 cm^2 V^{-1} s^{-1} at $T = 5$ K and a progressive decrease at higher temperatures (inset of Fig. 5). This is in good agreement with the values of mobility obtained from the magnetoresistance analysis of $BaFe_2As_2$ in the semimetal scenario [15,44]. Remarkably, this average mobility is strongly reduced upon electron doping

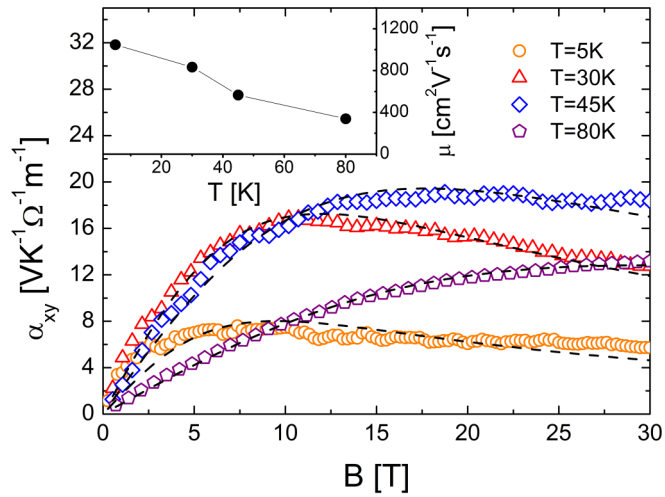

FIG. 6. Magnetic field dependences up to 30 T in the temperature range 5–80 K of α_{xy}. Dashed lines are the fitting curves of α_{xy} using Eq. (5). Inset: Temperature dependence of carrier mobility μ obtained by the fitting.

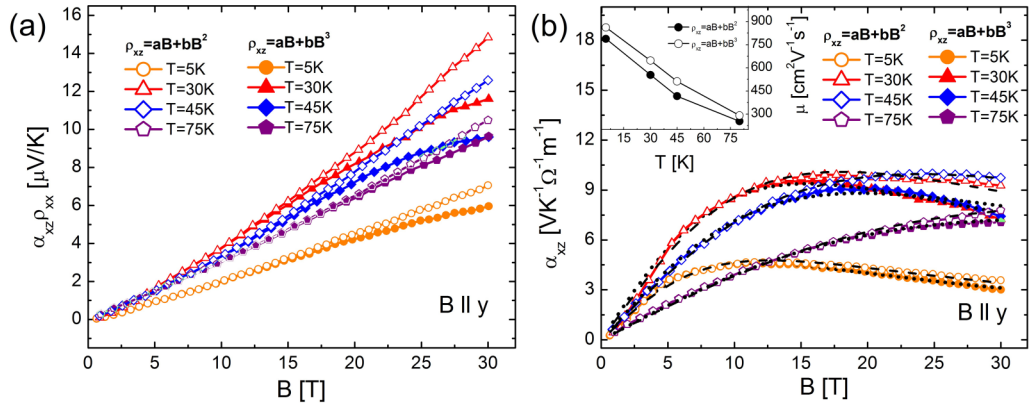

FIG. 7. Magnetic field dependences up to 30 T in the temperature range 5–80 K of $\alpha_{xz}\rho_{xx}$ (a) and α_{xz} (b) when ρ_{xz} is extrapolated up to 30 T using a polynomial of second (empty symbols) or third (filled symbols) order. Dashed and dotted lines in (b) are the fitting curves of α_{xz} using Eq. (5) when ρ_{xz} is extrapolated up to 30 T using a polynomial of second and third order, respectively. Inset of (b): Temperature dependence of carrier mobility obtained by the fitting.

with the simultaneous suppression of the magnetic phase, as the Dirac cones develop [44].

Taking into account the Shubnikov de Haas (SdH) oscillations measured in a $BaFe_2As_2$ crystal [45], we can assume that for $B\|z$ the electron γ pocket with the lowest effective mass gives the main contribution to α_{xy}. The γ-pocket carrier density has been estimated [45] to be $3\times10^{19}\,\mathrm{cm}^{-3}$ and considering the coefficient $c\sim1$, from the fit coefficients A at $T=5$, 30, and 45 K, we estimate E_F in the range $\sim$11–25 meV. Being aware that it only represents a qualitative approximation, it is interesting to notice that the proposed value for E_F comes out tiny and consistent with the size of the electron γ pocket estimated from SdH oscillations [45]. Remarkably, this pocket has been located in a position of the band structure where Dirac cones with E_F of $\sim$10 meV have been experimentally confirmed by ARPES [12,13] and infrared studies [7] in the AFM phase of $BaFe_2As_2$.

Oganesyan and Ussishkin predicted that in the presence of Dirac cones, the nodal point of which is close enough to the Fermi level (i.e., very small E_F), a giant Nernst coefficient can be determined by an anomalously high α_{xy} [46]. Moreover, Morinari *et al.* demonstrated that the contribution of chiral Dirac fermions could be dominant in thermoelectric transport properties of iron-based parent compounds even if they are minor carriers [11]. Giant Nernst coefficients in the similar compounds $EuFe_2As_2$ and $CaFe_2As_2$ have indeed been reported [19,28]. All these evidences suggest that the giant α_{xy}, responsible for the large Nernst effect that we observe experimentally, is plausibly determined by the Dirac cone band, which indeed perfectly fulfils the required condition of high mobility and small Fermi energy.

We now turn to the $B\|y$ configuration. We have experimental data of ρ_{xz} up to 9 T, but we do not have any indication whether with increasing field it remains negative or changes in sign as ρ_{xy} does. In [22] we report two different extrapolations of experimental ρ_{xz} data from 9 to 30 T using a polynomial of second and third order to take into account different magnetic field dependencies. The second-order polynomial simulates a nonmonotonic B dependence of ρ_{xz} which, however, does not change sign up to 30 T, whereas the third-order polynomial reproduces a sign change from negative to positive, but this occurs at fields much higher than in the case of ρ_{xy}. In [22] we show that notwithstanding the two very different extrapolations the term which contains ρ_{xz} in Eq. (2) ($\alpha_{xx}\rho_{xz}$) is negligible and thus the term $\alpha_{xz}\rho_{xx}$ in N_{xz} can be reliably discussed.

Figure 7(a) shows the magnetic field dependence of $\alpha_{xz}\rho_{xx}$ up to 30 T in the temperature range 5–80 K with ρ_{xz} extrapolated up to 30 T using a polynomial of second (empty symbols) or third (filled symbols) order. In both cases $\alpha_{xz}\rho_{xx}$ reaches values up to 12–14 μV/K so that it is possible to conclude that this term determines the giant N_{xz} [Fig. 3(d)], as already observed for $\alpha_{xy}\rho_{xx}$ with respect to N_{xy}. In Fig. 7(b) we show the magnetic field dependence of α_{xz} up to 30 T in the temperature range 5–80 K, for the two ρ_{xz} extrapolations. Comparing it with Fig. 6 it is interesting to note that α_{xz} is a factor 2 smaller than α_{xy} and their magnetic field dependence is pretty similar, i.e., well described by Eq. (5). We interpolated our α_{xz} data using Eq. (5) as a fitting function [dashed and dotted lines in Fig. 7(b)] and we extracted the mobility μ as a fit parameter, obtaining values up to $825\pm35\,\mathrm{cm}^2\,\mathrm{V}^{-1}\,\mathrm{s}^{-1}$ at $T=5$ K and a progressive decrease by raising the temperature. Furthermore, the A values [Eq. (5)] resulting from the fitting are compatible with those previously obtained for $B\|z$.

In the $B\|y$ configuration, where cross-plane transport comes into play, we extract an effective carrier mobility which is slightly lower than for in-plane transport ($B\|z$), but still high enough to be compatible with a Dirac dispersion. This observation points to a possible three-dimensional nature of DFs in this compound, providing a clue in the still open issue of two- or three-dimensional character of DFs in the parent compounds of iron-based superconductors, addressed both by theory [7,47,48] and experiments [7,49].

Contrary to N_{xz}, both the terms which compose S_{xx} [Eq. (1)] are strongly affected by the ρ_{xz} uncertainty, so that their magnetic field dependence cannot be univocally disentangled [22]. In particular, the different behavior exhibited by ΔS_{xx} for $B\|z$ and $B\|y$, reported in Figs. 3(a) and 3(c), respectively, may arise from a B anisotropy of ρ_{xy} and ρ_{xz}. On the other hand, another possible anisotropic contribution comes from the magnon drag mechanisms, which should influence

the longitudinal term $\alpha_{xx}\rho_{xx}$ of S_{xx} only when $B\|y$, as it has been discussed in [38]. (See [22] for further information.) These aspects are demanding for ρ_{xz} measurement up to high B, in order to shed light both on the anisotropy of ρ_{ij} and on the magnon drag contribution to S_{xx}.

IV. CONCLUSION

In conclusion, we measured the longitudinal and transverse electric and thermoelectric properties in magnetic fields up to 30 T for two field directions in a $BaFe_2As_2$ single crystal. By carrying out a simultaneous quantitative analysis of all these properties, which are mutually intertangled in the diffusive transport equations, we demonstrated the possibility of extracting information on band structure and dispersion, as well as on multiple physical mechanisms in play other than diffusive motion of carriers. Indeed, the anomalous field dependence and the anisotropy of the thermoelectric properties turn out to be distinctive and reveal key features of microscopic mechanisms. Specifically, we identified the presence of high mobility carriers, compatible with the existence of DFs in the band structure, from the giant magnitude of the off-diagonal terms of the thermoelectric tensor α_{xy} and α_{xz}. Moreover, from the anisotropic thermoelectric response with respect to the direction of the applied field, we found possible evidence of the 3D nature of DFs in $BaFe_2As_2$.

Finally, our results suggest that the simultaneous analysis of longitudinal and transverse electric and thermoelectric properties is a powerful investigation tool of diffusive transport, which relies on, rather than being hindered by, the complex temperature and magnetic field dependence exhibited by real compounds, where multiple mechanisms may play a role, such as multiband character, presence of bands with different dispersion, dimensionality, and transport properties.

ACKNOWLEDGMENTS

We acknowledge Nicodemo Magnoli and Alessandro Braggio for fruitful discussions. We acknowledge the support of PRIN 2012X3YFZ2 and the FP7 European project SUPER-IRON (Grant No. 283204). Part of this work has been performed at the High Field Magnet Laboratory Nijmegen (HFML-RU/FOM), member of the European Magnetic Field Laboratory.

[1] N. P. Armitage, E. J. Mele, and A. Vishwanath, Rev. Mod. Phys. **90**, 015001 (2018).
[2] B. Yan and C. Felser, Annu. Rev. Condens. Matter Phys. **8**, 337 (2017).
[3] K. S. Novoselov, A. K. Geim, S. V. Morozov, D. Jiang, M. I. Katsnelson, I. V. Grigorieva, S. V. Dubonos, and A. A. Firsov, Nature (London) **438**, 197 (2005).
[4] Y. Feng, D. Liu, B. Feng, X. Liu, L. Zhao, Z. Xie, Y. Liu, A. Liang, C. Hu, Y. Hu, S. He, G. Liu, J. Zhang, C. Chen, Z. Xu, L. Chen, K. Wu, Y.-T. Liu, H. Lin, Z.-Q. Huang, C.-H. Hsu, F.-C. Chuang, A. Bansil, and X. J. Zhou, Proc. Natl. Acad. Sci. USA **113**, 14656 (2016)
[5] Y. L. Chen, J. G. Analytis, J.-H. Chu, Z. K. Liu, S.-K. Mo, X. L. Qi, H. J. Zhang, D. H. Lu, X. Dai, Z. Fang, S. C. Zhang, I. R. Fisher, Z. Hussain, and Z.-X. Shen, Science **325**, 178 (2009).
[6] D. Hsieh, D. Qian, L. Wray, Y. Xia, Y. S. Hor, R. J. Cava, and M. Z. Hasan, Nature (London) **452**, 970 (2008).
[7] Z.-G. Chen, Luyang Wang, Yu Song, Xingye Lu, Huiqian Luo, Chenglin Zhang, Pengcheng Dai, Zhiping Yin, Kristjan Haule, and Gabriel Kotliar, Phys. Rev. Lett. **119**, 096401 (2017).
[8] J. Park, G. Lee, F. Wolff-Fabris, Y. Y. Koh, M. J. Eom, Y. K. Kim, M. A. Farhan, Y. J. Jo, C. Kim, J. H. Shim, and J. S. Kim, Phys. Rev. Lett. **107**, 126402 (2011).
[9] P. Tang, Q. Zhou, G. Xu, and Shou-Cheng Zhang, Nat. Phys. **12**, 1100 (2016).
[10] J. Paglione and R. L. Greene, Nat. Phys. **6**, 645 (2010).
[11] T. Morinari, E. Kaneshita, and T. Tohyama, Phys. Rev. Lett. **105**, 037203 (2010).
[12] Y. Kim, H. Oh, C. Kim, D. Song, W. Jung, B. Kim, H. J. Choi, C. Kim, B. Lee, S. Khim, H. Kim, K. Kim, J. Hong, and Y. Kwon, Phys. Rev. B **83**, 064509 (2011).
[13] P. Richard, K. Nakayama, T. Sato, M. Neupane, Y.-M. Xu, J. H. Bowen, G. F. Chen, J. L. Luo, N. L. Wang, X. Dai, Z. Fang, H. Ding, and T. Takahashi, Phys. Rev. Lett. **104**, 137001 (2010).
[14] I. Pallecchi, F. Bernardini, F. Caglieris, A. Palenzona, S. Massidda, and M. Putti, Eur. Phys. J. B **86**, 338 (2013).
[15] K. K. Huynh, Y. Tanabe, and K. Tanigaki, Phys. Rev. Lett. **106**, 217004 (2011).
[16] I. Pallecchi, F. Bernardini, M. Tropeano, A. Palenzona, A. Martinelli, C. Ferdeghini, M. Vignolo, S. Massidda, and M. Putti, Phys. Rev. B **84**, 134524 (2011).
[17] T. Terashima, H. T. Hirose, D. Graf, Y. Ma, G. Mu, T. Hu, K. Suzuki, S. Uji, and H. Ikeda, Phys. Rev. X **8**, 011014 (2018).
[18] I. Pallecchi, F. Caglieris, and M. Putti, Supercond. Sci. Technol. **29**, 073002 (2016).
[19] M. Matusiak, Z. Bukowski, and J. Karpinski, Phys. Rev. B **83**, 224505 (2011).
[20] S. Ishida, T. Liang, M. Nakajima, K. Kihou, C. H. Lee, A. Iyo, H. Eisaki, T. Kakeshita, T. Kida, M. Hagiwara, Y. Tomioka, T. Ito, and S. Uchida, Phys. Rev. B **84**, 184514 (2011).
[21] M. A. Tanatar, E. C. Blomberg, A. Kreyssig, M. G. Kim, N. Ni, A. Thaler, S. L. Bud'ko, P. C. Canfield, A. I. Goldman, I. I. Mazin, and R. Prozorov, Phys. Rev. B **81**, 184508 (2010).
[22] See Supplemental Material at http://link.aps.org/supplemental/10.1103/PhysRevB.98.155116 for magnetic susceptibility measurement, electric resistivity, interpolated data of longitudinal and transverse resistivity, temperature dependence of the Nernst coefficient, temperature dependence of R_H, and the analysis of Seebeck and Nernst versus B, when $B\|y$, which includes [S1, S2, S3]; [S1] G. M. Zhang *et al.*, EPL **86**, 37006 (2009); [S2] R. Klingeler *et al.*, Phys. Rev. B **81**, 024506 (2010); [S3] L. Wei-Yong *et al.*, Chinese Phys. B **19**, 087403 (2010).
[23] J.-H. Chu, J. G. Analytis, D. Press, K. De Greve, T. D. Ladd, Y. Yamamoto, and I. R. Fisher, Phys. Rev. B **81**, 214502 (2010).
[24] E. D. Mun, S. L. Bud'ko, N. Ni, A. N. Thaler, and P. C. Canfield, Phys. Rev. B **80**, 054517 (2009)
[25] S. Arsenijevic, R. Gaál, A. S. Sefat, M. A. McGuire, B. C. Sales, D. Mandrus, and L. Forró, Phys. Rev. B **84**, 075148 (2011).

[26] A. F. May, M. A. McGuire, J. E. Mitchell, A. S. Sefat, and B. C. Sales, Phys. Rev. B **88**, 064502 (2013).

[27] Y. J. Yan, X. F. Wang, R. H. Liu, H. Chen, Y. L. Xie, J. J. Ying, and X. H. Chen, Phys. Rev. B **81**, 235107 (2010).

[28] M. Matusiak, M. Babij, and T. Wolf, Phys. Rev. B **97**, 100506(R) (2018).

[29] In our experimental configuration for $B \| y$ [see Fig. 1(b)], the Seebeck coefficient is measured in the direction perpendicular to B. In agreement with [23], with increasing field, more domains with the orthorhombic a axis aligned perpendicular to the B direction would appear. Therefore, the contribution of S_a is expected to overcome the one of S_b (where S_b and S_a are the Seebeck coefficients along the b and the a axis, respectively) [28].The in-plane Seebeck anisotropy in $BaFe_2As_2$ in the considered temperature range ($T < 80$ K) comes out to be around 43% with $|S_b| > |S_a|$. Thus, if the detwinning is dominant we should expect a decrease of the total measured S coefficient with increasing B: Considering a change in the twin population of about 15% at 15 T [23], we estimated a reduction in the Seebeck effect with a maximum value of about 0.1 μV/K around 30 K. In contrast, at the same temperature and field, we measure S as high as 1.5 μV/K, that is ten times higher than the expected value. In the $B \| y$ configuration, the Nernst voltage is measured in the z direction (c axis), as represented in Fig. 1(b). Therefore, the detwinning should not influence this measurement.

[30] Taking into account the in-plane anisotropy of the resistivity which in [20] is reported to be as low as 4% at 5 K, similarly to the Seebeck coefficient [29], we evaluated that the detwinning effect at 5 K and 15 T is of the order of 0.7%.

[31] J. M. Ziman, *Principles of the Theory of Solids* (Cambridge University, Cambridge, England, 1972).

[32] L. J. van der Pauw, Philips Res. Rep. **16**, 1871961 (1961).

[33] K. Behnia, J. Phys.: Condens. Matter **21**, 113101 (2009).

[34] K. Behnia and H. Aubin, Rep. Prog. Phys. **79**, 046502 (2016).

[35] E. H. Sondheimer, Proc. R. Soc. A **193**, 484 (1948).

[36] Given that $\rho_{xx}\alpha_{xx} \simeq \alpha_{xx}/\sigma_{xx} \propto 1/\sigma_{xx}(\partial\sigma_{xx}/\partial\varepsilon)|_{\varepsilon=\mathrm{EF}} \propto (\partial \ln \sigma_{xx}/\partial\varepsilon)|_{\varepsilon=\mathrm{EF}}$, in the presence of a not negligible magnetoresistance, this term is not sizeably affected.

[37] G. N. Grannemann and L. Berger, Phys. Rev. B **13**, 2072 (1976).

[38] F. Caglieris, A. Braggio, I. Pallecchi, A. Provino, M. Pani, G. Lamura, A. Jost, U. Zeitler, E. Galleani D'Agliano, P. Manfrinetti, and M. Putti, Phys. Rev. B **90**, 134421 (2014).

[39] M. Matusiak, T. Plackowski, Z. Bukowski, N. D. Zhigadlo, and J. Karpinski, Phys. Rev. B **79**, 212502 (2009).

[40] H. Q. Yuan, L. Jiao, F. F. Balakirev, J. Singleton, C. Setty, J. P. Hu, T. Shang, L. J. Li, G. H. Cao, Z. A. Xu, B. Shen, and H. H. Wen, arXiv:1102.5476.

[41] F. Caglieris, A. Leveratto, I. Pallecchi, F. Bernardini, M. Fujioka, Y. Takano, L. Repetto, A. Jost, U. Zeitler, and M. Putti, Phys. Rev. B **96**, 104508 (2017).

[42] T. Liang, Q. Gibson, J. Xiong, M. Hirschberger, S. P. Koduvayur, R. J. Cava, and N. P. Ong, Nat. Comm. **4**, 2696 (2013).

[43] A. A. Abrikosov, *Fundamental of the Thory of Metals* (Elsevier, Amsterdam, 1988).

[44] H.-H. Kuo, J.-H. Chu, S. C. Riggs, L. Yu, P. L. McMahon, K. De Greve, Y. Yamamoto, J. G. Analytis, and I. R. Fisher, Phys. Rev. B **84**, 054540 (2011)

[45] T. Terashima, N. Kurita, M. Tomita, K. Kihou, C.-H. Lee, Y. Tomioka, T. Ito, A. Iyo, H. Eisaki, T. Liang, M. Nakajima, S. Ishida, S. I. Uchida, H. Harima, and S. Uji, Phys. Rev. Lett. **107**, 176402 (2011).

[46] V. Oganesyan and I. Ussishkin, Phys. Rev. B **70**, 054503 (2004).

[47] Z. P. Yin, K. Haule, and G. Kotliar, Nat. Phys. **7**, 294 (2011).

[48] Z. P. Yin, K. Haule, and G. Kotliar, Nat. Mater. **10**, 932 (2011).

[49] M. Nakajima, M. Nagafuchi, and S. Tajima, Phys. Rev. B **97**, 094511 (2018).